Microreactors

DOI: 10.1002/anie.201004217

Chaotically Accelerated Polymerase Chain Reaction by Microscale Rayleigh–Bénard Convection**

*Radha Muddu, Yassin A. Hassan, and Victor M. Ugaz**

Chemical processes can unfold in surprising and unpredictable ways when performed in the presence of chaotic advection. But the underlying interplay between reaction and flow remains poorly understood, and the "design" rules needed to rationally apply these effects are largely unknown. Here, we show how this fundamental coupling can be harnessed in flow fields generated by microscale thermal convection to achieve rapid biochemical replication of DNA through the polymerase chain reaction (PCR)—a process that involves cyclically heating and cooling an aqueous reagent cocktail to temperatures corresponding to denaturation of the double-stranded (ds) template DNA (ca. 95 °C), annealing of primers at specific locations on the denatured single-stranded fragments (ca. 50–60 °C), and enzyme-catalyzed extension to synthesize the complementary strands (ca. 72 °C). Although the reactor configuration to execute convective PCR is conceptually simple (i.e., the classical Rayleigh–Bénard system in which a fluid is heated from below in a cylindrical chamber of height h and diameter d; Figure 1), remarkably complex flow phenomena can emerge when convective turbulence occurs even though the flow is inertially laminar.[1] These states can be mapped in a parameter space governed by the aspect ratio (h/d) and the Rayleigh number ($Ra = [g\beta(T_2 - T_1)h^3]/\nu\alpha$; where β is the fluid's thermal expansion coefficient, g is gravitational acceleration, T_1 and T_2 are the temperatures of the top (cool) and bottom (hot) surfaces, respectively, h is the height of the fluid layer, α is the thermal diffusivity, and ν is the kinematic viscosity).

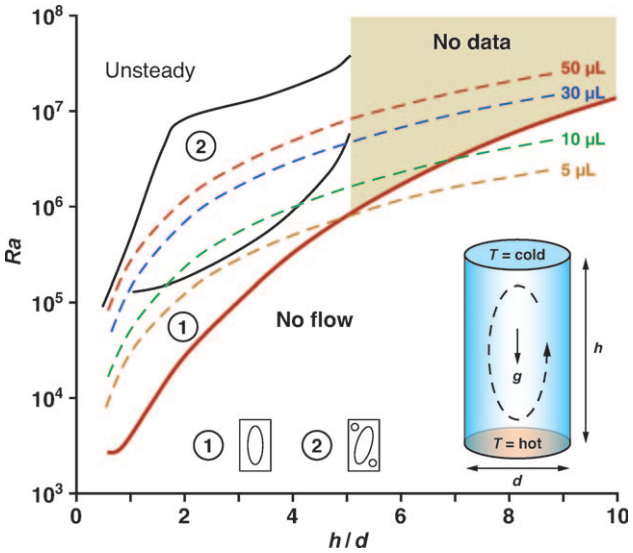

Figure 1. Microscale thermal convection generates a multiplicity of flow regimes at $h/d > 1{:}1$. The critical Rayleigh number Ra_c associated with the onset of convective motion scales as $(h/d)^4$ (solid red curve[1b,4]). Flows immediately above Ra_c are characterized by stable non-axisymmetric motion (rising on one side of the chamber and falling on the other; regime ①), with the emergence of complex 3D flow paths and/or multiple convection cells at higher Ra (regime ②), ultimately giving way to unsteady convective turbulence. At present there is insufficient data to infer how these regimes extrapolate to $h/d > 5{:}1$ (shaded region). Curves of constant reactor volume (dashed lines) indicate realistically accessible states under PCR conditions ($\Delta T = 35$ °C is imposed between the upper and lower surfaces).

In previous efforts to replicate DNA using microscale thermal convection, it has been assumed that flow fields that promote uniform pseudo-2D circulation between the reactor's top and bottom surfaces are most desirable because reagents are inherently exposed to well-defined cyclic temperature profiles.[2] These states occur near the boundary associated with the onset of flow (i.e., immediately above the solid red line in Figure 1), as evident in computational simulations at $h/d = 9{:}1$ ($Ra = 2.66 \times 10^7$; Figure 2a). Characteristics of the resulting flow trajectories can be visualized when the computed streamtrace data are used to plot excursions across the reactor midplane as a function of time in terms of a Poincaré map.[3] This analysis shows that the fluid elements follow tightly closed paths whose loci generate distinct Kolmogorov–Arnold–Moser (KAM) curves. Consequently, reagents are exposed to a thermal profile characterized by quasiperiodic oscillation between upper and lower extremes, as seen when temperature versus time is plotted following a fluid element. In contrast, a much different flow

[*] Prof. V. M. Ugaz
Artie McFerrin Department of Chemical Engineering
Texas A&M University, 3122 TAMU
College Station, TX 77843 (USA)
Fax: (+1) 979-458-1002
E-mail: ugaz@tamu.edu
R. Muddu, Prof. Y. A. Hassan
Department of Mechanical Engineering
Texas A&M University
College Station, TX 77843 (USA)
Prof. Y. A. Hassan
Department of Nuclear Engineering
Texas A&M University
College Station, TX 77843 (USA)

[**] This work was supported by the US National Science Foundation (NSF) under grant CBET-0933688 and the US National Institutes of Health (NIH) under grant NIH R01-HG003364. We gratefully thank T. Ragucci, B. Watkins, S. Wong, J. Mueller, and B. Wallek at Lynntech, Inc. for technical assistance and many helpful discussions.

Supporting information for this article is available on the WWW under http://dx.doi.org/10.1002/anie.201004217.

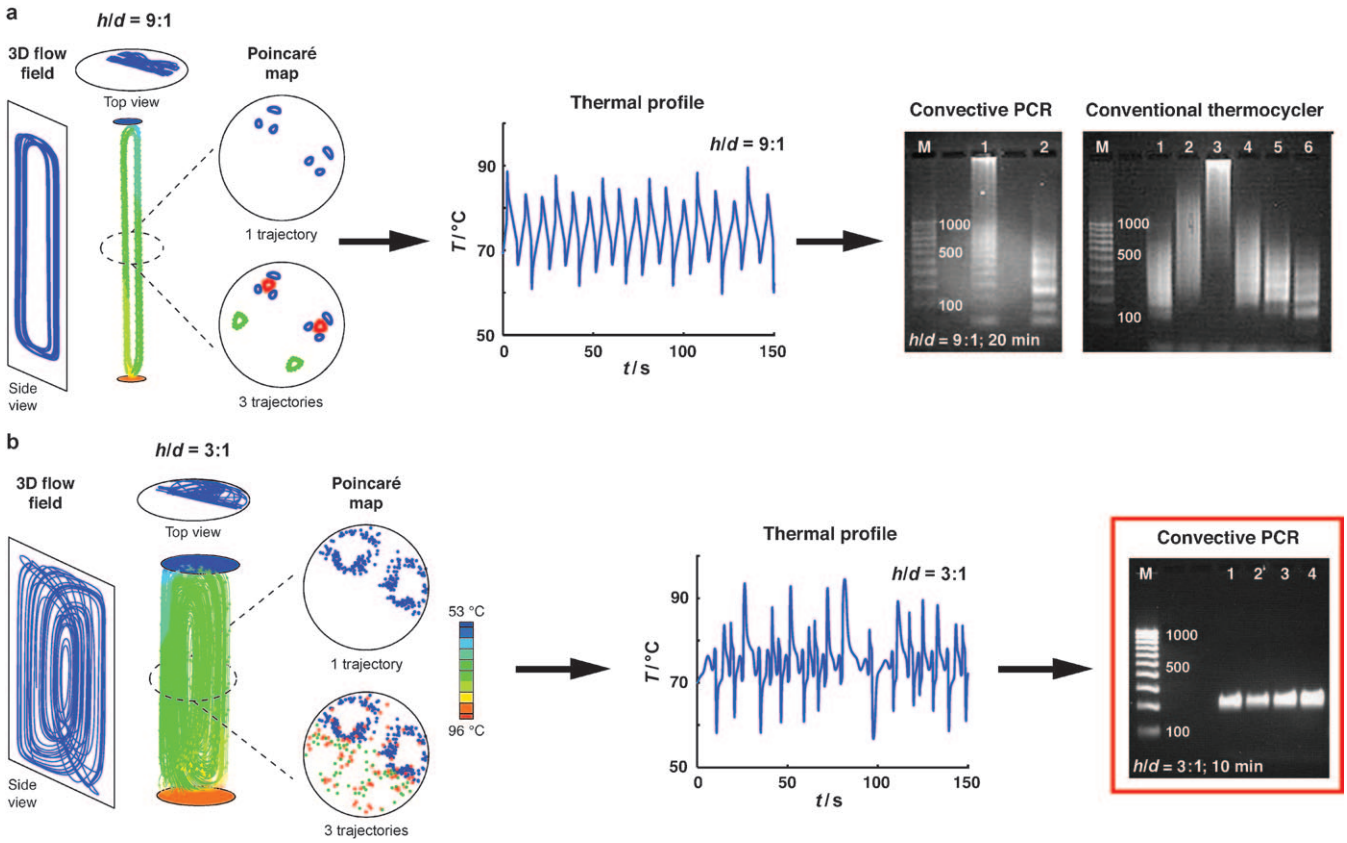

Figure 2. Computational simulations of microscale thermal convection and corresponding PCR results in aspect ratios of a) $h/d = 9{:}1$ (38.2 μL, $Ra = 2.66 \times 10^7$) and b) $h/d = 3{:}1$ (18.5 μL, $Ra = 1.45 \times 10^6$) with temperatures of 53 and 96 °C imposed at the top and bottom surfaces, respectively. A representative trajectory followed by a passive tracer, advected in the 3D flow field, is shown for each geometry along with top- and side-view projections of the path. Excursions across the reactor midplane ($h/2$) are used to construct Poincaré maps for the trajectory shown (blue points) and for two additional trajectories (red and green points). At $h/d = 9{:}1$, the flow field transports reagents along pseudo-2D trajectories that are essentially closed loops, as evident by quasiperiodic oscillation in the corresponding plot of temperature versus time following a fluid element. A more complex chaotic flow field is generated at $h/d = 3{:}1$, which disrupts the periodicity in the thermal profile. The chaotic nature of the convective flow field at $h/d = 3{:}1$ greatly accelerates DNA replication through the PCR flow, as evident by strong products observed by gel electrophoresis after only 10 minutes of reaction time (M: 100 bp ladder, lanes 1-4: products from four parallel reactions). In contrast, the reaction must be run for at least 20 minutes to obtain visible products at $h/d = 9{:}1$, and multiple bands are evident that indicate nonspecific replication (M: 100 bp ladder, lanes 1 and 2: products from two parallel reactions). Similar multiple product bands also appear in a conventional thermocycler when different pairs of denaturing (T_d) and annealing (T_a) temperatures are applied to mimic thermal profiles encountered at different locations within the reactor at $h/d = 9{:}1$ (M: 100 bp ladder, lanes 1–6: reaction products where T_d [°C]/T_a [°C] = 91.6/58.4, 92.5/57.5, 93.7/56.3, 94.9/55.1, 96/54, and 96.5/53.5, respectively).

field emerges when the reactor's shape is shorter and wider ($h/d = 3{:}1$, $Ra = 1.45 \times 10^6$; Figure 2b). Here, fluid elements follow complex 3D trajectories that no longer produce well-defined KAM boundaries in the Poincaré map but instead yield a broadly distributed pattern consistent with divergence of neighboring flow paths and emergence of chaos—a feature that acts to disrupt periodicity in the accompanying thermal profile.

These observations lead to seemingly contradictory conclusions about optimal reactor design for convective PCR. On one hand, flow fields at about $h/d = 9{:}1$ intuitively seem most desirable because there is a uniform pseudo-2D circulation between the cylinder's top and bottom surfaces that exposes reagents to a well-defined cyclic temperature history, which mirrors flow fields applied in conventional thermocycling instruments. But the quasiperiodic fluid motion in this regime also offers little opportunity for exchange between optimal thermal profiles (oscillating between the widest temperature extremes at the reactor's top and bottom surfaces) and the much larger ensemble of remaining trajectories that are much less favorable (localized closer to the center and therefore unable to fully access optimal temperatures; Movie 1 in the Supporting Information). On the other hand, $h/d = 3{:}1$ does not appear to be a good choice because the thermal profile is more disordered and lacks the distinct periodicity evident at $h/d = 9{:}1$. However, the chaotic nature of the collective fluid motion is potentially beneficial because individual flow trajectories are no longer locked-in to follow closed loops, thereby enabling much more of the total reagent volume to experience optimal temperatures and become engaged in the reaction (Movie 2 in the Supporting Information).

To ascertain which of these competing considerations most strongly influences the reaction, we used both of the above-mentioned geometries to perform convective PCR replication of a 295 base pair (bp) target associated with the β-actin gene from a human genomic DNA template. Unex-

pectedly, we routinely achieved amplification of the correct target in only 10 minutes at $h/d = 3{:}1$ (Figure 2b), while the same reaction at $h/d = 9{:}1$ exhibited an initial 15–20 minutes lag period[5] after which at least 20–30 minutes were required before comparable products became evident (Figure 2a). It is likely that the reaction at $h/d = 3{:}1$ proceeds even faster than the 10 minutes timescale shown in Figure 2b, but our experimental platform did not allow us to explore this limit because the approximately 1 minute transient period to establish and stop the flow becomes a nontrivial fraction of the total reaction time.

Reaction specificity was also much greater at $h/d = 3{:}1$ and a single PCR product was obtained, while multiple nonspecific products were generated at $h/d = 9{:}1$, consistent with the hypothesis that the closed-flow streamlines trap fluid elements within unfavorable thermal trajectories, thereby exposing reagents to a multiplicity of different temperature profiles depending on their location within the reactor. We illustrated this effect by using a conventional thermocycler to mimic conditions in the convective reactor at $h/d = 9{:}1$ through a series of individual PCR experiments, each involving a different set of annealing and denaturing temperatures (Figure 2a). These thermal profiles are distributed over a wide temperature range, representative of complete circulation between the top and bottom surfaces (53 °C annealing, 96 °C denaturing), to a narrower range corresponding to flow trajectories encountered closer to the center (58 °C annealing, 91 °C denaturing). Different sets of nonspecific products are replicated depending on the applied temperatures, thus bolstering our hypothesis that the multiple products observed in the convective system at $h/d = 9{:}1$ represent integrated effects over the entire ensemble of individual thermal profiles (both favorable and unfavorable) distributed throughout the reactor volume. The chaotic fluid motion at $h/d = 3{:}1$ therefore appears to enable the reaction to proceed faster and with greater specificity by exposing a much greater fraction of reagents to favorable thermal conditions.

We applied a kinetic model to better understand the implications of this coupling between flow and reaction.[6] In particular, we wanted to be certain that the enhanced reaction efficiency observed at $h/d = 3{:}1$ was indeed attributable to the chaotic nature of the flow field, or if it could instead reflect a beneficial effect because the residence time at intermediate temperatures has increased, which is associated with extension (Figure 2b)—the rate-limiting step in PCR. These calculations yield a characteristic trend of exponential growth in dsDNA concentration, from which a doubling time can be extracted as a parameter that represents the timescale associated with execution of a complete temperature cycle (Figure 3; also see the Supporting Information). Based on this analysis, the doubling time at $h/d = 9{:}1$ (11.6 s) is predicted to be much more rapid than at $h/d = 3{:}1$ (27.3 s), which sharply contradicts our experimental observations. The discrepancy between experimental results (showing that the reaction proceeds at least twice as fast at $h/d = 3{:}1$ than at $h/d = 9{:}1$) and kinetic simulations (which predict the opposite) imply that the chaotic flow field's ability to collectively expose a large fraction of the reagent volume to favorable thermal profiles at $h/d = 3{:}1$ is highly desirable. Thus, while the orderly

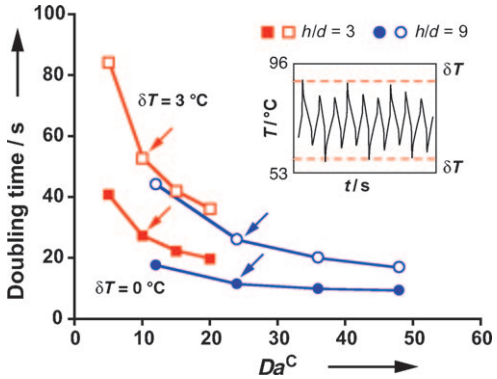

Figure 3. Evolution of the characteristic doubling time with the convective Damköler number Da^C obtained using a kinetic model with the thermal profiles in Figure 2 as inputs. Under ideal conditions (i.e., reagents are optimally transported through all temperature zones; $\delta T = 0$ °C, lower curves), the reaction is predicted to proceed much faster at $h/d = 9{:}1$ ($Da^C = 24$, blue arrows) than at $h/d = 3{:}1$ ($Da^C = 10$, red arrows), the opposite of what is observed experimentally. This trend is maintained in response to perturbations away from ideal temperature profile conditions ($\delta T = 3$ °C, upper curves), except that doubling times increase over the entire Da^C range.

flow at $h/d = 9{:}1$ appears to be a more logical choice (and, therefore, previously thought to represent an optimal design[2]), the chaotic advection introduced at $h/d = 3{:}1$ counterintuitively dominates reaction kinetics on a global scale.

Despite their importance, few convenient model systems exist to study chemical reactions in 3D chaotic flows.[7] Rayleigh–Bénard convection at $h/d > 1{:}1$ fulfills this need by providing a robust platform to probe a wide variety of 3D flows, incorporating features ranging from quasiperiodic motion to full-blown chaos.[1a] To highlight the spectrum of accessible flow states, we performed simulations by applying three different temperature gradients between the top and bottom surfaces of 30 μL reactors at $h/d = 3{:}1$ ($\Delta T = 5$, 35, and 100 °C) and $h/d = 8{:}1$ ($\Delta T = 35$, 50, and 200 °C; Figure 4). Decreasing ΔT from PCR conditions ($\Delta T = 35$ °C) to 5 °C at $h/d = 3{:}1$ induces a transition from chaotic trajectories in Figure 2b to a 2D circulatory profile, with quasiperiodic characteristics evident in the emergence of KAM boundaries in the Poincaré map. Conversely, increasing ΔT from 35 to 100 °C causes the flow field to become even more disordered, accompanied by signatures of multiple convection loop structures, and in qualitative agreement with the flow-regime boundaries previously identified at $h/d < 5{:}1$.[1b] A similar cascade is evident at $h/d = 8{:}1$, where closed-loop quasiperiodic motion gives way to chaotic advection when ΔT is increased to 200 °C. An analogous transition is also initiated by moving from $h/d = 8{:}1$ to 3:1 at constant Ra. These results suggest the capability to select from a broad range of flow states to apply a prescribed chaotic component to the fluid motion, thereby making it possible to rationally design reactors in which chaos is introduced in a controlled way and tailored to enhance a wide variety of chemical processes.

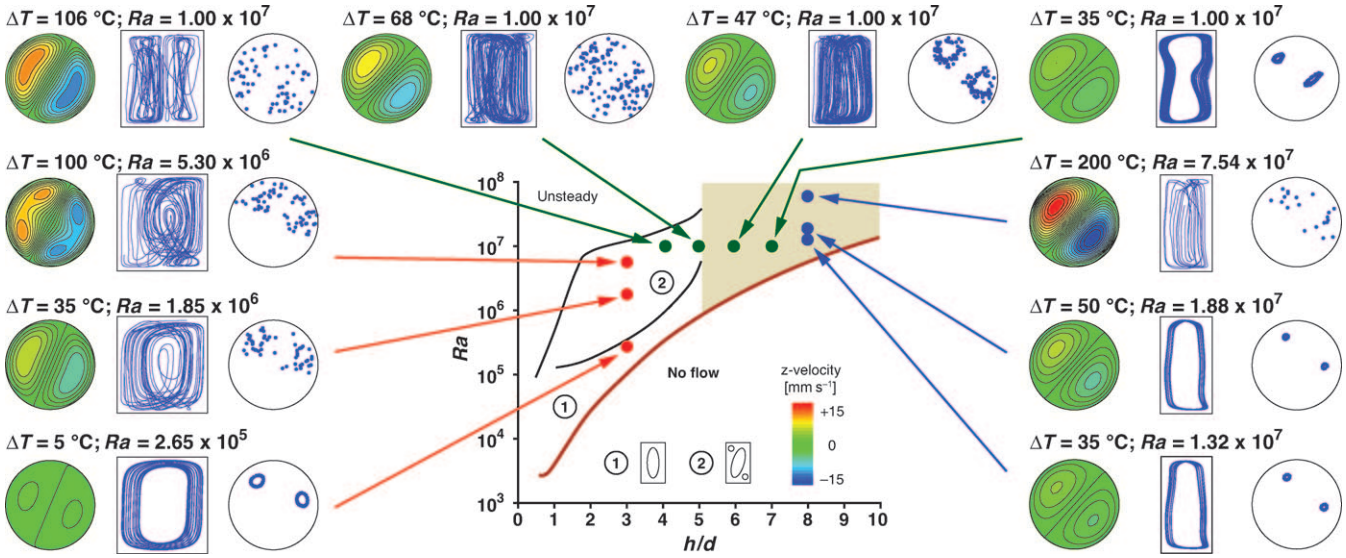

Figure 4. Convective flows at $h/d > 1{:}1$ incorporate a chaotic component that can be precisely tuned over a wide range. Computational simulations reveal that chaotic effects become prominent as *Ra* is increased at constant h/d (red and blue points) and as h/d is decreased at constant *Ra* (green points). At ten different conditions in the parameter space, we show a plot of the vertical (*z*-direction) velocity distribution over a cross-sectional plane at $h/2$ (left), a side-view projection of a representative passive tracer trajectory (middle), and the corresponding Poincaré map at $h/2$ (right). *Ra* values at a given h/d are selected by changing the temperature difference ΔT applied between the upper and lower surfaces (volume held constant at 30 μL).

Experimental Section

Experiment conditions: Overall design and operation of the convective thermocycling instrument has been described in detail previously.[5] Cylindrical reactor wells were constructed by machining arrays of holes in polycarbonate blocks to achieve the desired aspect ratios ($h/d = 9{:}1$ $h = 15.9$ mm, $d = 1.75$ mm, 38.2 μL volume; $h/d = 3{:}1$ $h = 6.02$ mm, $d = 1.98$ mm, 18.5 μL volume). PCR experiments were performed to replicate a 295 base pair β-actin target from a human genomic DNA template using Thermococcus kodakaraenis (KOD) DNA polymerase. A typical 100 μL reaction mixture contained 10 μL of buffer no. 1, 6 μL of 25 mM $MgCl_2$, 10 μL of deoxynucleotidetriphosphates (dNTPs; 2 mM each), 41.2 μL of deionized (DI) water, 10 μL of β-actin probe, 10 μL of β-actin forward primer, 10 μL of β-actin reverse primer, 2 μL of human genomic template DNA (10 ng μL^{-1}), and 0.8 μL of KOD DNA polymerase (2.5 units μL^{-1}). The enzyme, buffer (buffer no. 1), $MgCl_2$, and dNTPs were supplied with the KOD DNA polymerase kit (cat. no. 71085–3; Novagen). The primers, probe, and template DNA were supplied with the TaqMan β-actin Control Reagents kit (cat. no. 401846; Applied Biosystems). The reactions shown in Figure 3c were performed using a conventional thermocycler (T-Gradient; Biometra) following a two-temperature protocol (15 s denaturing, 30 s annealing) for 30 cycles.

Computational fluid dynamics (CFD) analysis: Flow simulations were performed under conditions matching the PCR experiments in reactor geometries of $h/d = 3{:}1$ and 9:1 (annealing and denaturing temperatures of 53 and 96 °C were imposed, respectively). A cylindrical geometry was created for each of these cases using GAMBIT and meshed with hexahedral elements. The corresponding flow and thermal fields were then computed using FLUENT (version 6.0.12) with a three-dimensional, laminar, steady-state model. The working fluid was defined as water with Boussinesq properties evaluated at 95 °C, and an insulating boundary condition was applied along the sidewalls of the cylinder. Gravity was included as a body force and a converged solution was obtained by using a second-order upwind discretization scheme for the momentum and energy balances, a PRESTO! scheme for pressure, and a SIMPLE scheme for pressure–velocity coupling. Analysis of flow trajectories was performed using Tecplot. See the Supporting Information for additional details.

Kinetic reaction model: A kinetic model was applied which represents the important features of convective PCR by a simplified framework expressed in terms of kinetics associated with 1) denaturing: dsDNA → 2ssDNA (rate constant k_d); 2) annealing: ssDNA → aDNA (rate constant k_a); and 3) extension: aDNA → dsDNA (rate constant k_e).[6] These expressions serve as inputs to a dimensionless reaction–diffusion Equation (1),

$$\frac{\partial c_i}{\partial t} + \mathbf{v}\cdot\nabla c_i = \frac{\mathrm{D}c_i}{\mathrm{D}t} = \frac{1}{Pe}\nabla^2 c_i + Da^c r_i \qquad (1)$$

where c_i are the concentrations of the individual species (dsDNA, ssDNA, aDNA), $\mathbf{v}$ represents the velocity field, $Pe = h\bar{u}/D$ is the Péclet number expressing the relative timescales of flow and diffusion (h is the cylinder height of 6.02 and 15.9 mm at $h/d = 3{:}1$ and 9:1, respectively), $\bar{u}$ is a characteristic velocity taken to be the magnitude averaged over the flow trajectory (3.3 and 3.7 mm s^{-1} at $h/d = 3{:}1$ and 9:1, respectively), $D = 10^{-7}$ cm^2 s^{-1} is the mass diffusion coefficient of DNA, fluid properties are evaluated at 95 °C), and Da^C is the convective Damköhler number $k^*h/\bar{u}$, which expresses the relative timescales of flow and chemical reaction (k^* is a characteristic reaction rate constant taken to be 5.564 s^{-1}, consistent with available kinetic data[8]). The rates of change in concentration r_i of each species c_i are determined from the stoichiometric balances [Eq. (2a–c)],

$$r_{ss} = 2\kappa_d f_d(\mathbf{x},t)c_{ds} - \kappa_a f_a(\mathbf{x},t)c_{ss} \qquad (2a)$$

$$r_a = \kappa_a f_a(\mathbf{x},t)c_{ss} - \kappa_e f_e(\mathbf{x},t)c_a \qquad (2b)$$

$$r_{ds} = \kappa_e f_e(\mathbf{x},t)c_a - \kappa_d f_d(\mathbf{x},t)c_{ds} \qquad (2c)$$

where κ_i are dimensionless reaction rate constants (i.e., k_i/k^*) and f_i is a mapping function applied to localize each step of the reaction within its respective temperature zone.[6a] The temperature versus time data shown in Figure 2 express a Lagrangian representation of the local environment surrounding a fluid element when it experiences advection along its flow trajectory, and can thus be applied directly to evaluate the rates of change associated with each individual species concentration $\mathrm{D}c_i/\mathrm{D}t$ using Equations (1) and (2a–c) (the $1/Pe$ term in Equation (1) can be neglected under the

conditions of interest here, where $Pe \approx 10^7$.). These calculations yield kinetic data that follow a characteristic trend of exponential growth in dsDNA concentration, from which a doubling time can be extracted to yield a parameter that represents the timescale associated with execution of a complete temperature cycle. See Supporting Information for additional details.

Received: July 9, 2010
Revised: January 4, 2011
Published online: February 25, 2011

Keywords: analytical methods · biochemistry · chaos · DNA replication · microreactors

[1] a) F. Heslot, B. Castaing, A. Libchaber, *Phys. Rev. A* **1987**, *36*, 58705873; b) G. Müller, G. Neumann, W. Weber, *J. Cryst. Growth* **1984**, *70*, 78 – 93.

[2] M. Krishnan, V. M. Ugaz, M. A. Burns, *Science* **2002**, *298*, 793.

[3] a) J. M. Ottino, *The Kinematics Of Mixing: Stretching, Chaos, And Transport*, Cambridge University Press, Cambridge, **1989**; b) H. J. Kim, A. Beskok, *J. Micromech. Microeng.* **2007**, *17*, 2197 – 2210.

[4] a) G. S. Charlson, R. L. Sani, *Int. J. Heat Mass Transfer* **1971**, *14*, 2157 – 2160; b) I. Catton, D. K. Edwards, *AIChE J.* **1970**, *16*, 594 – 601.

[5] a) M. Krishnan, N. Agrawal, M. A. Burns, V. M. Ugaz, *Anal. Chem.* **2004**, *76*, 6254 – 6265; b) V. M. Ugaz, M. Krishnan, *JALA* **2004**, *9*, 318 – 323.

[6] a) J. W. Allen, M. Kenward, K. D. Dorfman, *Microfluid. Nanofluid.* **2009**, *6*, 121 – 130; b) E. Yariv, G. Ben-Dov, K. D. Dorfman, *Europhys. Lett.* **2005**, *71*, 1008 – 1014.

[7] a) G. O. Fountain, D. V. Khakhar, J. M. Ottino, *Science* **1998**, *281*, 683 – 686; b) J. P. Gollub, P. E. Arratia, *Phys. Rev. Lett.* **2006**, *96*, 024501.

[8] S. Mehra, W. S. Hu, *Biotechnol. Bioeng.* **2005**, *91*, 848 – 860.

